Self-Assembled Monolayers of Ruthenium and Osmium Bis-Terpyridine Complexes—Insights of the Structure and Interaction Energies by Combining Scanning Tunneling Microscopy and Electrochemistry

E. Figgemeier,*,†,|| L. Merz,‡ B. A. Hermann,‡ Y. C. Zimmermann,§ C. E. Housecroft,§ H.-J. Güntherodt,‡ and E. C. Constable*,§,⊥

University of Uppsala, Department of Physical Chemistry, P.O. Box 532, 75121 Uppsala, Sweden, University of Basel, Department of Physics - Condensed Matter, Klingelbergstr. 82, 4056 Basel, Switzerland, and University of Basel, Department of Inorganic Chemistry, Spitalstr. 51, 4056 Basel, Switzerland

Received: July 15, 2002; In Final Form: November 14, 2002

Self-assembled monolayers of $[Ru(terpy)(terpy\text{-}py)]^{2+}$ and $[Os(terpy)(terpy\text{-}py)]^{2+}$ salts (terpy is 2,2′:6′,2″-terpyridine and terpy-py is 4′-(4-pyridyl)-2,2′:6′,2″-terpyridine) on platinum were investigated by means of STM and electrochemistry. The STM experiments reveal that the species within the monolayer are ordered in a hexagonal array. This information was utilized together with the scan rate dependency of the peak current density (j_p) of potential sweep experiments to calculate interaction energies within the monolayer. Significantly, the repulsive interactions within the monolayers of 2,2′:6′,2″-terpyridine complex are greater than those observed with analogous 2,2′-bipyridine species. This results in a lower overall surface coverage, an ordered structure where each particle has 6 closest neighbors, and a shift of the redox potentials toward more positive values with the terpy complexes. Also, a correlation between the solvent dielectric constant and the interaction energies could be established, reflecting the different ability of the solvent to screen charges depending upon its polarity.

Introduction

Self-assembled monolayers of redox active complexes have attracted significant interest during the past decade.[1−6] This is in part due to the accessibility of new experimental techniques for studying these systems such as scanning tunneling microscopy (STM)[7,8] or high-speed voltammetry[3] and it is also driven by the likely role of monolayers in future applications such as molecular electronics[9] or contemporary developments such as the dye-sensitized nano-structured solar cell (NSC). In particular, in the NSC the microscopic properties of surface bound species on a molecular level are difficult to investigate, because the surface area is very large[10] and therefore transport processes, monolayer assembling, and structure are complicated and not well understood. In this context, fundamental studies of monolayers on well-defined surfaces such as gold or platinum gives valuable information about electron-transfer rates and mechanisms, intermolecular interactions, and redox behavior.

The electrochemical properties of self-assembled monolayers of ruthenium and osmium complexes on platinum and gold surfaces have been of central interest. A number of studies relating to electron transfer[3−6] and self-assembly processes[11−13] of osmium oligopyridine and related complexes have been reported. The choice of metal center in these studies is primarily dictated by the accessibility of the osmium(II)/(III) redox process (∼0.5 V vs ferrocene−ferrocenium) compared to the Ru analogues.

Although these studies were made primarily upon 2,2′-bipyridine (bpy) complexes, metal complexes with 2,2′:6′,2″-terpyridine (terpy) ligands are attracting increasing interest as components of multimetallic arrays due to favorable geometric properties. Indeed, the inherent linearity of complexes with 4′-substituted terpy ligands make them also very interesting candidates for purpose built surface architectures.[8] In the present paper we report the electrochemical properties and structure as probed by STM of self-assembled monolayers $[Ru(terpy)(terpy\text{-}py)]^{2+}$ and $[Os(terpy)(terpy\text{-}py)]^{2+}$ salts (Figure 1). These complexes were chosen because they represent prototype species for anchoring linearly developed polynuclear complexes to metal surfaces through the pendant 4-pyridyl substituent. The synthesis and interaction of such polynuclear species will be published in due course.[14]

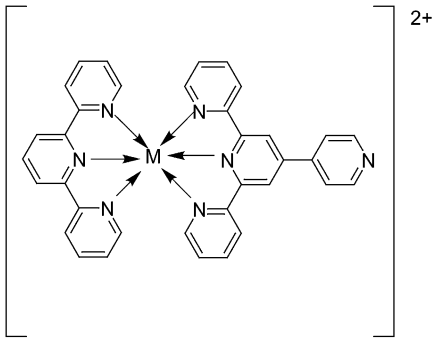

Figure 1. Structural image of $[M(terpy)(terpy\text{-}py)]^{2+}$ with M = Ru, Os.

Experimental Section

Reagents. For the electrochemical experiments, acetonitrile (Fluka) with a water content lower than 0.001% stored over molecular sieve was used. Dichloromethane (Aldrich) was distilled and also stored over molecular sieve. The supporting

* Corresponding authors.
† University of Uppsala, Department of Physical Chemistry.
‡ University of Basel, Department of Physics - Condensed Matter.
§ University of Basel, Department of Inorganic Chemistry.
|| E-mail: egbert.figgemeier@fki.uu.se.
⊥ E-mail: e.c.constable@bham.ac.uk.

10.1021/jp026522d CCC: $25.00 © 2003 American Chemical Society
Published on Web 01/09/2003

electrolyte for electrochemical experiments in acetonitrile and dichloromethane was tetrabutylammonium hexafluorophosphate ($TBAPF_6$, Aldrich) and was dried in a vacuum oven at 120 °C for at least 24 h before use. $LiClO_4$ (99.9% Aldrich) was used for the electrochemistry in aqueous solutions. For the synthetic procedures, commercially available chemicals were of reagent grade and used without further purification. The compounds [Ru(terpy)Cl_3)],[15] [Os(terpy)Cl_3),][16] and 4′-(4-pyridyl)-2,2′:6′,2″-terpyridine[17] were prepared according to literature methods.

Synthesis of [Ru(terpy)(terpy-py)][PF_6]$_2$. A suspension of [Ru(terpy)Cl_3] (0.020 g, 0.045 mmol) and 4′-(4-pyridyl)-2,2′:6′,2″-terpyridine (0.014 g, 0.045 mmol) in ethylene glycol (5 mL) together with two drops of *N*-ethylmorpholine was heated to reflux in microwave oven (800 W) for 10 min. A solution of saturated aqueous ammonium hexafluorophosphate (25 mL) was then added to the dark-red solution, and the precipitate was collected by filtration over Celite and dissolved in acetonitrile. The solvent was evaporated in vacuo and the residue was purified by column chromatography (silica/acetonitrile-saturated aqueous potassium nitrate−water, 7:1.5:0.5). To the major red-orange fraction, an excess of ammonium hexafluorophosphate was added and the solution wasreduced in volume. The precipitate was collected by filtration over Celite, washed with acetonitrile, and evaporated to dryness to afford [Ru(terpy)(terpy-py)][PF_6]$_2$ (0.029 g, 68%) as a red-orange powder. ^{1}H NMR (250 MHz, CD_3CN, δ): 9.07 (2H, s, $H_{pyterpy}3'$), 9.00 (2H, m, H_m), 8.79 (2H, d, J = 8.3 Hz, H3′), 8.68 (2H, d, J = 8.2 Hz, $H_{pyterpy}3/3''$), 8.53 (2H, d, J = 8.2 Hz, H3/3″), 8.46 (1H, t, J = 8.3 Hz, H4′), 8.16 (2H, m, H_o), 8.02−7.92 (4H, m, H4/4″, $H_{pyterpy}4/4''$), 7.43−7.39 (4H, m, H6/6″, $H_{pyterpy}6/6''$), 7.25−7.17 (4H, m, H5/5‴, $H_{pyterpy}5/5''$). IR (KBr, cm^{-1}): 3426m, 3107w, 1628w, 1601m, 1476w, 1465w, 1449m, 1429w, 1409m, 1385m, 1030w, 841s, 789w, 769m, 558s. UV/VIS (CH_3CN): λ_{max}/nm (ϵ/dm^3 mol^{-1} cm^{-1}) 272.8 (71600), 308.9 (76400), 482.3 (27100). FAB-MS: *m*/*z* 790 ([M−PF_6]$^+$), 645 ([M−2 PF_6]$^{2+}$). Anal. Calcd. for $C_{35}H_{25}N_7RuP_2F_{12}$ (934.6): C 44.9, H 2.7, N 10.5. Found: C 44.7, H 3.0, N 10.3%.

Synthesis of [Os(terpy)(terpy-py)][PF_6]$_2$. A suspension of [Os(terpy)Cl_3] (0.020 g, 0.037 mmol) and 4′-(4-pyridyl)-2,2′:6′,2″-terpyridine (0.012 g, 0.037 mmol) in ethylene glycol (5 mL) together with two drops of *N*-ethylmorpholine was heated to reflux in a microwave oven (800 W) for 10 min. Saturated aqueous ammonium hexafluorophosphate (25 mL) was then added to the dark solution, and the precipitate was collected by filtration over Celite and dissolved in acetonitrile. The solvent was evaporated in vacuo and the residue was purified by column chromatography (silica/acetonitrile-saturated aqueous potassium nitrate−water, 7:1.5:0.5). To the major brown fraction an excess of ammonium hexafluorophosphate was added and the solution was reduced in volume. The precipitate was collected by filtration over Celite, dissolved in acetonitrile, and evaporated to dryness to afford [Os(terpy)(terpy-py)][PF_6]$_2$ (0.012 g, 31%) as a dark-brown powder. ^{1}H NMR (250 MHz, CD_3CN, δ): 9.09 (2H, s, $H_{pyterpy}3'$), 8.97 (2H, m, H_m), 8.81 (2H, d, J = 8.0 Hz, H3′), 8.67 (2H, d, J = 8.2 Hz, $H_{pyterpy}3/3''$), 8.51 (2H, d, J = 8.2 Hz, H3/3″), 8.13 (2H, m, H_o), 7.99 (1H, t, J = 8.0 Hz, H4′), 7.89−7.78 (4H, m, H4/4″, $H_{pyterpy}4/4''$), 7.30−7.27 (4H, m, H6/6″, $H_{pyterpy}6/6''$), 7.18−7.09 (4H, m, H5/5‴, $H_{pyterpy}5/5''$). IR (KBr, cm^{-1}): 3403w, 3117w, 1636m, 1603w, 1450m, 1428m, 1385s, 1357m, 1029w, 839s, 788w, 766m, 558s. UV/VIS (CH_3CN): λ_{max}/nm (ϵ/dm^3 mol^{-1} cm^{-1}) 273.0 (53300), 312.8 (61500), 482.7 (21000), 662.5 (5000). ES-MS: *m*/*z* 880 ([M−PF_6]$^+$). Anal. Calcd. for $C_{35}H_{25}N_7OsP_2F_{12}$ (1023.8): C 41.1, H 2.5, N 9.6. Found: C 40.9, H 2.6, N 9.8%.

Electrochemistry. Cyclic voltammetry was performed using a CH Instruments Model 660 Electrochemical workstation and a conventional three-electrode cell with a BAS Ag/AgCl electrode as reference. Microelectrodes were fabricated from platinum wires (Goodfellow Metals Ltd.) of radii between 5 and 25 μm by sealing them into soft glass using a procedure described previously by Forster and Faulkner.[4] Microdisk electrodes were exposed by removing excess glass using 600 grit emery paper followed by successive polishing with 12.5, 5, 1, 0.3, and 0.05 μm alumina. The polishing material was removed between changes of particle size by sonicating the electrodes in deionized water for at least 5 min. The polished electrodes were electrochemically cleaned by cycling in 0.5 M H_2SO_4 between potential limits chosen to first oxidize and then to reduce the surface of the platinum electrode. Excessive cycling was avoided in order to minimize the extent of surface roughening. The real, or microscopic, surface area of microelectrodes and the macroelectrodes was found by calculating the charge under the oxide or hydrogen adsorption−desorption peaks. Before removing the electrode from the cell, the potential was then held in the double layer region at a sufficiently negative value to ensure complete reduction of any surface oxide. Finally, the electrode was cycled between −0.300 and 0.700 V in 0.1 M $LiClO_4$ until hydrogen desorption was complete. Typically the surface roughness factor was between 1.5 and 2.0. RC cell time constants were between 0.03 and 3 μs, depending on the electrode radius and the supporting electrolyte concentration.

The electrochemical behavior of the self-assembled monolayers was measured in acetonitrile with tetrabutylammonium hexafluorophosphate (0.1 M) as the supporting electrolyte. All potentials given are quoted vs the ferrocene−ferrocenium redox couple.

Scanning Tunneling Microscopy. A Nanoscope III (Digital Instruments Santa Barbara, CA) with a "low current converter" (room temperature in air) was employed in ambient conditions for the STM investigations. Platinum substrates were made from cleaned, rolled, polished, and annealed Pt wire (Johnson Matthey). All investigations were restricted to the Pt(100) surface (checked by investigations of the surface morphology which was previously correlated with X-ray analysis[18]).

Preparation of Monolayers. The freshly prepared platinum foils or electrodes were immersed into an aqueous acetone solution of the complexes for at least 1 h. In this time the complexes spontaneously formed adsorbed monolayers. The surfaces were thoroughly rinsed with the solvent to remove nonbound material before performing electrochemistry or STM experiments, respectively.

Results and Discussion

Electrochemical Response. The electrochemistry of [Ru(terpy)(terpy-py)]$^{2+}$ as well as [Os(terpy)(terpy-py)]$^{2+}$) in acetonitrile solution with $TBAPF_6$ (0.1 M) as supporting electrolyte is characterized by the appearance of one signal in the oxidative region of the potential window (0.92 and 0.60 V vs ferrocene−ferrocenium). On the other side, four reduction peaks were observed for each complex (−1.56 V, −1.86 V, −2.24 V, and −2.61 V for [Ru(terpy)(terpy-py)]$^{2+}$ and −1.53 V, −1.84 V, −2.21 V, and −2.58 V for [Os(terpy)(terpy-py)]$^{2+}$) (Figure 2). These redox processes were assigned to the successive reduction of the two terpy ligands, assuming that each ligand can be reduced twice within the potential window. Presumably, the first peak belongs to the reduction of the pyridine substituted terpy ligand, since the additional aromatic ring lowers the π^* lowest unoccupied molecular orbital due to an increased conjugation.

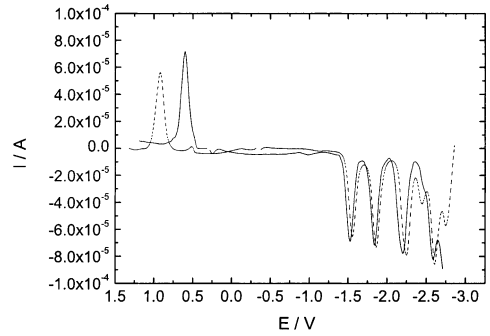

Figure 2. Differential pulse voltammograms of [Os(terpy)(terpy-py)]-$[PF_6]_2$ (solid line) and [Ru(terpy)(terpy-py)]$[PF_6]_2$ (dashed line) in solution (vs ferrocene−ferrocenium). Both voltammograms were recorded in acetonitrile and $TBAPF_6$ (0.1 M) as the supporting electrolyte.

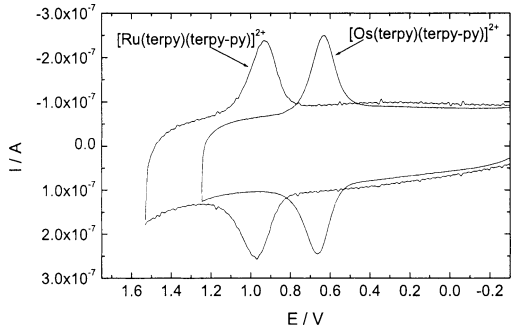

Figure 3. Cyclic voltammograms of monolayers of [Os(terpy)(terpy-py)]$[PF_6]_2$ and [Ru(terpy)(terpy-py)]$[PF_6]_2$ on a platinum microelectrode ($r = 25$ μm) at 500 V s^{-1} (vs ferrocene−ferrocenium). Both voltammograms were recorded in acetonitrile and $TBAPF_6$ (0.1 M) as the supporting electrolyte.

This is supported by less negative reduction potentials for the symmetric [Ru(terpy-py)$_2$]$[PF_6]_2$ complex in comparison to [Ru(terpy)$_2$]$[PF_6]_2$.[19] The typical electrochemical responses of the self-assembled monolayers obtained by dipping electrodes in solutions of [Ru(terpy)(terpy-py)]$[PF_6]_2$ and [Os(terpy)(terpy-py)]$[PF_6]_2$ measured in acetonitrile with 0.1 M $TBAPF_6$ as supporting electrolyte are presented in Figure 3. In each case, fully reversible redox behavior assigned to the metal(II)/(III) processes are observed. The peak-to-peak separation between the current maximum (minimum) of the anodic and the cathodic potential, ΔE_p, was less than 20 mV at moderate scan rates (<1000 V/s utilizing a 25 μm platinum electrode). However, at higher scan rates ΔE_p increases in agreement with the predicted influence of the heterogeneous electron-transfer kinetics on the voltammetric response.[20] The peak currents of the monolayers show a linear increase with the scan rate (Figure 4) as is predicted for such systems and in contrast to nonbound redox active material where the peak current is primarily influenced by diffusion.[20] The oxidation potentials for the ruthenium and osmium species were found to be 0.97 and 0.65 V, respectively, when bound to the surface. The reductions could not be observed when measuring the self-adsorbed monolayers without desorption. The full width at half-maximum ($\Delta E_{p,1/2}$) of the electrochemical responses of monolayers of both complexes is between 150 and 160 mV. The saturation surface coverages (Γ_s) of the Ru complex is 2.5($\pm$ 0.2) $\times$ 10^{-11} mol cm^{-2} and 3.3($\pm$ 0.2) $\times$ 10^{-11} mol cm^{-2} for the Os homologue as calculated from the charge under the oxidation and reduction peaks of the cyclic voltammograms.

STM Imaging. After applying the procedure for self-assembling of monolayers (see experimental part) on a freshly prepared platinum foil for [Ru(terpy)(terpy-py)]$[PF_6]_2$, the samples were dried and investigated by STM at room temperature in air. Typically, the images showed bright spots against a dark background. The spots are ordered in a 2-dimensional closed packed symmetry, with each particle having six nearest neighbors. The average distance between adjacent spots was determined to be 2.9 nm, while a spot has a radius of approximately 0.55 nm, which indicates a rather loose packing. This large molecule-to-molecule distance could be caused by a repulsive interaction between the molecules. Assuming that one spot corresponds to one molecule, a surface coverage of 2.2 $\times$ 10^{-11} mol cm^{-2} can be calculated. An example of such an image is given in Figure 5. It proved difficult to obtain stable images; even though the complex is expected to form a reasonably strong bond to the substrate, it appears that the molecules have a high flexibility and a large rotational freedom (this mobility has been described previously for similar complexes[7]). At a scan speed of 240 nm/s, we probably image an overlay of statistically distributed positions for each molecule. An additional complication arises from the STM experiment itself; the STM tip has a finite width, preventing it from following the full surface of the molecules in the *z*-direction. The molecules appear spherical and the STM technique is not capable of giving submolecular resolution. Furthermore, the measurements were made in air, where no reconstructions of platinum are known and the obtained pattern was referenced to currently known reconstructions of the platinum surface observed in UHV—no matches were found. In no cases the untreated platinum surfaces show features such as those in Figure 5. The low applied bias-voltage and the fact that the complexes are rather loosely packed indicates that the STM images are of individual [Ru(terpy)(terpy-py)]$^{2+}$ cations in the monolayer. With this assumption, the calculated total surface coverage Γ_T (of 2.2 $\times$ 10^{-11} mol cm^{-2}) is within the experimental errors of these experiments, in excellent agreement with the electrochemically determined value (see above).

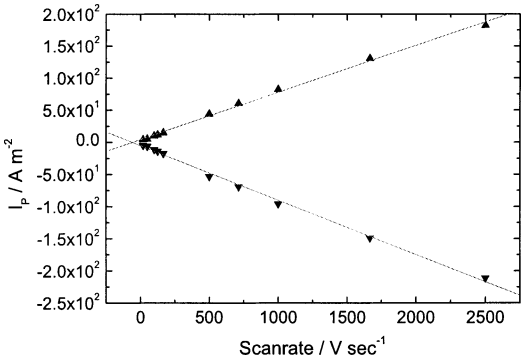

Figure 4. Example for the peak current density as a function of scan rate for a monolayer of [Ru(terpy)(terpy-py)]$(PF_6)_2$ on a platinum microelectrode ($r = 25$ μm). All voltammograms were recorded in acetonitrile and $TBAPF_6$ (0.1 M) as the supporting electrolyte.

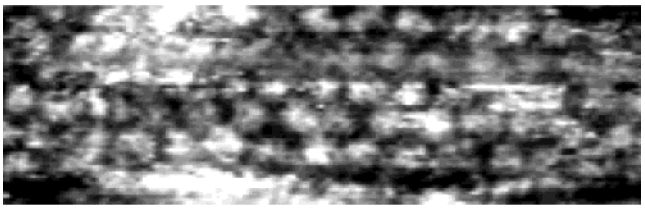

Figure 5. 14 nm $\times$ 45 nm STM image of a $[Ru(terpy)(terpy-py)]^{2+}$ monolayer on Pt(100). Tunneling parameters: $U_{bias} = 200$ mV, $I_t =$ 30 pA, scan speed = 240 nm/s, constant current mode.

Adsorption and Monolayer Structure. $\Delta E_{p,1/2}$ and Interaction Energies. Adsorption isotherms are utilized most com-

monly in order to understand the results of electrochemical investigations of redox active monolayers and to calculate free energies of adsorption (ΔG_i).[21,22] Most commonly, the Langmuir isotherm has been used—assuming no lateral interactions between the adsorbed species on the surface.[23] By doing so, a theoretical value of 90.6 mV for $\Delta E_{p,1/2}$ of a cyclic voltammogram for a one-electron redox process was predicted. Indeed, experimental values relatively close to 90.6 mV (between 100 and 110 mV) were taken as a strong indication that the molecules do not "feel" major forces between them. This was assumed for most self-assembled monolayers consisting of polypyridine complexes closely related to our compounds such as $[Ru(bpy)_2(Qpy)]^{2+}$ (Qpy is 2,2′:4,4″:4′4″-quarterpyridyl and bpy is 2,2′-bipyridyl)[24] or $[Os(bpy)_2(bpe)Cl]^+$ (bpe = *trans*-1,2-bis(4-pyridyl)ethylene).[25]

In our case, the assumption of no interactions between the adsorbed molecules does not hold since we determined values for $\Delta E_{p,1/2}$ of up to 160 mV for the Os and the Ru complex.

One option to take care of lateral interactions is to expand the Langmuir isotherm simply by an interaction parameter (g) leading to the Frumkin isotherm:[20]

$$\beta_i C_i = \frac{(\theta_i)}{1-\theta_i}\exp(g\theta_i) \tag{1}$$

where $\theta_i = \Gamma_i/\Gamma_s$, Γ_i is the surface concentration of the species i at the bulk concentration C_i, Γ_s is the saturation coverage and β_i is the adsorption coefficient which relates to the free energy of adsorption:

$$\beta_i = \exp(-\Delta G_i/RT) \tag{2}$$

From the above approach, a correlation between $\Delta E_{p,1/2}$ and the lateral interaction can be derived. Qualitatively, at values smaller than 90.6 mV, attractive interactions can be assumed, whereas at higher numbers the molecules are feeling repulsive forces. Therefore we can conclude that a rather strong repulsion dominates in our systems. However, the approach derived from the Frumkin isotherm assumes a completely random distribution of the adsorbed species and therefore does not take into account ordered structures within the monolayer despite lateral interactions. For our self-assembled monolayers we see very clearly such 2-dimensional ordering (Figure 5). Therefore we decided to employ a statistical mechanical treatment proposed by Matsuda et al.[26,27] which allows us to calculate interaction energies within the monolayer.

For a simple surface redox reaction ($R \rightleftharpoons O + ne^-$) Matsuda et al. derived an expression for the peak current density j_p of a potential sweep experiment:

$$(j_p)_a = -(j_p)_c = \frac{nF\Gamma_T(nF\upsilon/RT)}{4\{1-(z/2)(1-1/\epsilon)\}} \tag{3}$$

for $zln\{z/(z-2)\} \geq W/RT \geq zn\beta_r$, and

$$(j_p)_a = -(j_p)_c = \frac{nF\Gamma_T(nF\upsilon/RT)(1-\beta_r^2)}{4\{1-(z/2)(1-1/\beta_r)\}(1-\epsilon^2)} \tag{4}$$

for $W/RT < zln\beta_r$. where $(j_p)_a$ and $(j_p)_c$ are the anodic and the cathodic peak current densities, n is the number of electrons transferred in the reaction, F is the Faraday constant, R is the gas constant, T is the temperature in Kelvin, Γ_T is the total surface coverage, υ is the potential sweep rate, and ϵ is given by

$$\epsilon = \exp(W/zRT) \tag{5}$$

where z represents the number of nearest neighbors and W is the interaction energy which is defined by

$$W = (W_{RR} + W_{OO}) - W_{RO} \tag{6}$$

where W_{RR} is the interaction energy of reduced particles, W_{OO} of oxidized particles, and W_{OR} of pairs of oxidized and reduced species.

β is a function of the mole fractions of the oxidized and reduced species and ϵ. Without going into too many details, r indicates a solution for β in an algebraic equation of third order, appearing when deriving the above given equations. For further details, we refer to the original literature.[26,27]

In Figure 5 we clearly see that the number of nearest neighbors is 6. According to Matsuda et al. this gives us $\beta_r = 0.6943$ and therefore we get from eqs 3 and 4:

$$(j_p)_a = -(j_p)_c = \frac{nF\Gamma_T(nF\upsilon/RT)\epsilon}{4(3-2\epsilon)} \tag{7}$$

for $2.43 \geq W/RT \geq -2.19$, and

$$(j_p)_a = -(j_p)_c = \frac{nF\Gamma_T(nF\upsilon/RT)0.223}{4(1-\epsilon^2)} \tag{8}$$

for $W/RT < -2.19$.

Equations 7 and 8 represent linear relations between j_p and the scan rate υ with the slopes m_1 and m_2 given by

$$m_1 = \frac{n^2F^2\Gamma_T}{RT}\frac{0.223}{[4(3-2\epsilon)]} \tag{9}$$

and

$$m_2 = \frac{n^2F^2\Gamma_T}{RT}\frac{0.223}{[4(1-\epsilon^2)]} \tag{10}$$

respectively. After determining the slope of $j_p = f(\upsilon)$, we can calculate ϵ from eqs 9 and 10, which gives us W according to eq 5. The lateral interaction energies for our complexes were calculated and are listed in Table 1.

TABLE 1: Values for *W* of Ru and Os Complexes Calculated by Determining the Slope of $j_p = f(\upsilon)$ and Using Equations 9 and 10[a,b]

	W_a (kJ/mol)	W_c (kJ/mol)	W (kJ/mol)
$[Ru(terpy)(terpy\text{-}py)]^{2+}$	−5.9	−4.8	−5.35
$[Os(terpy)(terpy\text{-}py)]^{2+}$	−4.5	−4.3	−4.4
$[Os(bpy)_2(bpe)Cl]^+$	−3.8	−2.6	−3.2

[a] Measurements were recorded in acetonitrile with 0.1 M $TBAPF_6$ as the supporting electrolyte. [b] bpe = *trans*-1,2-bis(4-pyridyl)ethylene.

In Table 1 the values calculated from the cathodic (W_c) and the anodic (W_a) waves are listed as well as the average of both. It has to be noticed that the difference between W_c and W_a for $[Ru(terpy)(terpy\text{-}py)]^{2+}$ is significant. At this stage of the investigation the reason for this remains unclear. Further studies need to be performed to clarify this discrepancy. Nevertheless, going from $[Ru(terpy)(terpy\text{-}py)]^{2+}$ to its Os homologue is accompanied by a decrease of W by 1 kJ/mol. Taking the

TABLE 2: Values for *W* for Self-assembled Monolayers of [Os(terpy)(terpy-py)]$^{2+}$ in Different Solvents as a Function of the Dielectric Constant (ϵ_{eff})

solvent	W_a (kJ/mol)	W_c (kJ/mol)	W (kJ/mol)	ϵ_{eff}
H_2O	−0.6	−0.7	−0.65	80.1
CH_3CN	−4.5	−4.3	−4.4	38.8
CH_2Cl_2	−7.2	−5.7	−6.45	9.08

uncertainty of W_c into account, the difference might be smaller but nevertheless this fact shows that the effective charge seen by the environment of the adsorbed Os complex is lower than for the Ru one. This might be explained by the additional electron sphere of the Os-atom leading to a more efficient charge screening of the nucleus. To compare our bisterpy with previously published bpy complexes we also calculated *W* for $[Os(bpy)_2(bpe)Cl]^+$, which is a typical example for these kind of complexes published in many other contributions.[3,11,24] The values for the peak current densities were taken from an earlier investigation,[25] in which scan rate dependencies were utilized to determine electron-transfer rates. In a contribution by Hudson and Abruña[7] STM pictures were shown for $[Os(bpy)_2(dipy)Cl]PF_6$ (dipy is trimethylene-4,4′-bipyridine), which has a structure very similar to the complex listed in Table 1. These pictures are showing clearly that every complex molecule on the surface has 4 nearest neighbors. With this number, the same calculation according to Matsuda et al. can be performed as demonstrated for $z = 6$ and the values for *W* are also listed in Table 1. There is a significant difference for the interaction energies between our terpy complex and the bpy homologue as it was also predicted by the treatment with the Frumkin isotherm. In this context it is important to notice that species with a net charge of +2 like $[Os(bpy)_2py(p3p)]^{2+}$ (p3p is 4,4′-trimethylenedipyridine)[28] show the same values for $\Delta E_{p,1/2}$ as with only one charge like $[Os(bpy)_2(dipy)Cl]^+$. This is somewhat surprising because a negatively charged ion in the ligand sphere should screen one of the charges of the metal ion very efficiently. It should also be considered that the chloro ligand can be split off easily and be replaced by a neutral solvent molecule under room light conditions.[29] This therefore would lead as well to a 2+ species on the surface. Nevertheless, this gives rise to the conclusion that the ligand sphere when comparing terpy and bpy ligands is of decisive importance for the charge screening in polypyridine complexes bound to a surface. One possible explanation for this observation is the difference in geometry of the bpy and terpy complexes. Geometrical restrictions of the terdentating terpy ligands give rise to a much less efficient filling of the octahedral surface of the complex—virtually leaving gaps—than bidentating ligands are able to. Also, the σ-donation of a terpy ligand is disturbed by the geometrical restrictions of the terdentating ligand, because the overlap with the *d*-orbitals is weaker. We also determined *W* as a function of the solvent. Since the formal potential of the RuII/III couple is at the very edge of the potential window of water, this study was only performed with the Os complex. The results are summarized in Table 2 and plotted in Figure 6. The expected result is that the repulsive interactions depend linearly on the dielectric constant ϵ_{eff} which points at the different ability to screen charges by solvents of different polarity.

***E*$_p$ and Γ_T.** One obvious consequence of the relatively high repulsive interactions are the up to 4 times lower surface coverages of $[Ru(terpy)(terpy-py)]^{2+}$ and $[Os(terpy)(terpy-py)]^{2+}$ in comparison to bpy complexes bound to the surface. This poins out that the surface coverage is governed by electrostatic properties and not by steric interactions. Another result of the strong repulsive interactions is the more positive redox potential

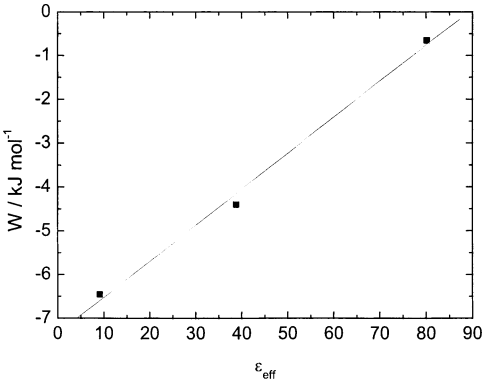

Figure 6. *W* for self-assembled monolayers of $[Os(terpy)(terpy-py)]^{2+}$ versus the dielectric constant ϵ_{eff} of the solvent.

for the complexes when bound to the surface in comparison to a solution of the species. This was predicted by the surface activity theory by Anson and Brown:[22]

$$E_p = E^0 + \frac{RT}{nF}(r_R - r_O)\Gamma_T \qquad (11)$$

where E_p is the formal potential of the surface bound species, $E°$ is the potential when there are no interaction forces, and r_R and r_O are the interaction parameters for the reduced and oxidized forms. A simple qualitative consideration shows that, according to Anson and Brown, with repulsive interaction we get negative values for r_R and r_O. Of course, r_O will have in this case a higher absolute value than r_R which gives us $E_P > E°$. This is in total agreement with our results, if we assume that the interaction forces in solution are much smaller than within a self-assembled monolayer due to the much larger average distance in solution. Thus, our solution potential is the equivalent to $E°$ in eq 11.

Conclusions and Outlook

We could show that the appearances of self-assembled monolayers consisting of $[Ru(terpy)(terpy-py)]^{2+}$ and $[Os(terpy)(terpy-py)]^{2+}$ differ in a few respects from the intensively studied analogue polypyridyl complexes of Ru and Os with bpy and chloro ligands. Most significantly, the repulsive interaction energies are significantly higher for the terpy complexes (indicated by the higher values of $\Delta E_{p,1/2}$ and calculated according to Matsuda et al.), which leads to a hexagonal 2-dimensional array, a lower surface coverage, and a positive shift of the redox potentials by 50 mV. Despite the thorough discussion of interaction energies and the STM image of adsorbed monolayers, the position of the counterions remains unclear. It can be speculated that they also maintain an ordered lattice within the monolayer. In this case, we would have a 2-dimensional analogue to a salt crystal of the type AB_2. Closely related to this is the open question, how far the complexes are moving apart at submonolayer coverages or "sticking" together due to the influence of the counterions. Cyclic voltammograms of submonolayers still showed values of $\Delta E_{p,1/2}$ much higher than 90.6 mV speaking in favor of islands of molecules. A detailed investigation of interaction energies at low values of Γ_T will give an answer to this question. This investigation should also consider the roughness of the surface, since a microscopically rough surface has kinks, steps, and terraces reducing the mobility of the adsorbed molecules resulting in higher interaction energies due to the reduced freedom to spread out on the surface. On the other side, this should not have an influence on the results

presented here, since only surfaces with a full coverage were considered. Nevertheless, we were able to show that terpy complexes bound to platinum surfaces are capable of building highly ordered structures due to a strong repulsion. Together with their inherent linearity, this might be a favorable property to build structures combined with functions on a molecular scale onto metal surfaces.

Acknowledgment. E.F. thanks Prof. Han Vos for the support and inspiring discussions and Prof. R. J. Forster for the opportunity to share his unmatched enthusiasm for the electrochemistry of self-assembled monolayers. The financial support by the NRP47 of the Swiss National Science Foundation is also acknowledged. B.A.H. gratefully acknowledges financial support from the Fonds der Chemie, Germany, and the BMBF, Germany.

References and Notes

(1) Forster, R. J.; Faulkner, L. R. *Anal. Chem.* **1995**, *67*, 1232−1239.
(2) Bretz, R. L.; Abruña, H. D. *J. Electroanal. Chem.* **1995**, *388*, 123−132.
(3) Forster, R. J.; Faulkner, L. R. *J. Am. Chem. Soc.* **1994**, *116*, 5444−5452.
(4) Forster, R. J.; Faulkner, L. R. *J. Am. Chem. Soc.* **1994**, *116*, 5453−5461.
(5) Finklea, H. O.; Yoon, K.; Chamberlain, E.; Allen, J.; Haddox, R. *J. Phys. Chem. B* **2001**, *105*, 3088−3092.
(6) Forster, R. J.; Keyes, T. E. *J. Phys. Chem. B* **2001**, *105*, 8829−8837.
(7) Hudson, J. E.; Abruña, H. D. *J. Phys. Chem.* **1996**, *100*, 1036−1042.
(8) Díaz, D. J.; Bernhard, S.; Storrier G. D.; Abruña, H. D. *J. Phys. Chem. B* **2001**, *105*, 8746−8754.
(9) Park, J.; Pasupathy, A. N.; Goldsmith, J. I.; Chang, C.; Yaish, Y.; Petta, J. R.; Rinkoski, M.; Sethna, J. P.; Abruña, H. D.; McEuen, P. L.; Ralph, D. C. *Nature* **2002**, *417*, 722−725.
(10) Hagfeldt, A.; Grätzel, M. *Acc. Chem. Res.* **2000**, *33*, 269−277.
(11) Acevedo, D.; Bretz, R. L.; Tirado, J. D.; Abruña, H. D. *Langmuir* **1994**, *10*, 1300−1305.
(12) Tirado, J. D.; Acevedo, D.; Bretz, R. L.; Abruña, H. D. *Langmuir* **1994**, *10*, 1971−1979.
(13) Campbell, J. L. E.; Anson, F. C. *Langmuir* **1996**, *12*, 4008−4014.
(14) Figgemeier, E.; Constable, E. C. To be published.
(15) Constable, E. C.; Cargill Thompson, A. M. W.; Tocher, D. A.; Daniels, M., A., M. *New J. Chem.* **1992**, *16*, 855−867.
(16) Buckingham, D. A.; Dwyer, F. P.; Sargeson, A. M. *Aust. J. Chem.* **1964**, *17*, 622.
(17) Constable E. C.; Cargill Thompson, A. M. W. *J. Chem. Soc., Dalton Trans.* **1992**, 2947−2950.
(18) Hubler, U. Ph.D. Thesis, 1999, Uni Basel.
(19) Constable, E. C.; Cargill Thompson, A. M. W. *J. Chem. Soc., Dalton Trans.* **1994**, 1409−1418.
(20) Bard, A. J.; Faulkner, L. R. *Electrochemical Methods, Fundamentals and Applications*; John Wiley & Sons: New York, 1980.
(21) Laviron, E. *J. Electroanal. Chem.* **1974**, *52*, 395.
(22) Brown, A. P.; Anson, F. C. *Anal. Chem.* **1977**, *49*, 1589.
(23) $\Delta G°$ values of about 50 kJ/mol were determined for monolayers consisting of complexes with bpy ligands. The evaluation of our adsorption data gave 59 kJ/mol for $\Delta G°$ which is higher but still a comparable value. Nothing else was expected despite all other discussed differences since for all cases the binding to the surface is done by a nitrogen atom of a pyridine ring.
(24) Forster, R. J.; Keyes, T. E. *J. Phys. Chem. B* **1998**, *102*, 10004−10012.
(25) Forster, R. J.; Figgemeier, E.; Loughman, P.; Lees, A.; Hjelm, J.; Vos, J. G. *Langmuir* **2000**, *16*, 7871−7875.
(26) Matsuda, H.; Aoki, K.; Tokuda, K. *J. Electroanal. Chem.* **1987**, *217*, 1−13.
(27) Matsuda, H.; Aoki, K.; Tokuda, K. *J. Electroanal. Chem.* **1987**, *217*, 15−32.
(28) Forster, R. J. *Inorg. Chem.* **1996**, *35*, 3394−3403.
(29) Forster, R. J.; Figgemeier, E.; Lees, A.; Hjelm, J.; Vos, J. G. *Langmuir* **2000**, *16*, 7867−7870.